Everything Else in the Spectrum

40

40.1. Fine Structure in the Ionization Edges 689
40.1.A. ELNES 689
40.1.B. EXELFS 694
40.2. The Low-Loss Spectrum 696
40.2.A. Plasmon Losses 696
40.2.B. Dielectric-Constant Determination 697
40.2.C. Band-Gap and Interband Transitions 698
40.2.D. Angle-Resolved EELS 698
40.3. Energy-Filtered and Spectrum Imaging 699
40.3.A. STEM Digital Imaging 700
40.3.B. TEM Analog Imaging 700

CHAPTER PREVIEW

The energy resolution of the magnetic prism spectrometer is very good, which means that the energy-loss spectrum contains a wealth of information about the specimen in addition to its basic elemental chemistry. In the previous chapter, we mentioned how we can learn about chemistry using ionization edges. Much of this chemical information is contained in fine-detail intensity variations at the ionization edges in the core-loss spectra termed *energy-loss near-edge structure* (ELNES) and *extended energy-loss fine structure* (EXELFS). From this fine structure, we can obtain information on how the ionized atom is bonded, the coordination of the atom, and its density of states. Furthermore, we can probe the distribution of other atoms around the ionized atom, i.e., the radial distribution function (RDF). Understanding these phenomena requires that we use certain concepts from atomic and quantum physics. The nonphysicist can skip some sections at this time and just concentrate on the results. The rewards of working through this topic will be an appreciation of some of the more powerful aspects of EELS.

> If high spatial resolution is important, you can't obtain this additional information by any other spectroscopic technique.

In addition to the extra information around the ionization edges, we can extract useful data from the low-loss region (<50 eV) of the spectrum. The predominant features in this part of the spectrum are the plasmon

D. B. Williams et al., *Transmission Electron Microscopy*

peaks, which represent the response of the weakly bound valence and conduction electrons to the high-energy incident electron. The plasmon response contains direct information about the free-electron density. In some binary free-electron alloys, plasmon-peak shifts reflect the composition of the specimen. Within the low-loss region, but separate from the intense plasmon peak, we can find intensity that is related to the dielectric constant of the specimen. Furthermore, we can discern certain inter/intraband transitions, especially in polymers, and we can measure directly the band gap of semiconductors and insulators. We also introduce briefly the effect of the angle of scatter of the energy-loss electrons, which can be studied using the DP.

We note how the intense nature of the EELS spectrum, due mainly to the very high collection efficiency of the spectrometer, permits EELS imaging. Energy-loss (or energy-filtered) images and DPs can be formed in two ways: slowly, quantitatively, and digitally, or rapidly and qualitatively in an analog fashion. The primary advantage of EELS imaging is that *all* the information available in the spectrum can be imaged and related to all the other diffraction and imaging techniques that come from the TEM.

Everything Else in the Spectrum

40

40.1. FINE STRUCTURE IN THE IONIZATION EDGES

We saw in Section 38.4 that the ionization edges have intensity variations both within about 30 eV of the onset of the edge (ELNES) and extending for several hundred eV as the edge intensity diminishes (EXELFS). This fine structure contains a wealth of useful information, but to understand its origins you have to use some ideas from quantum physics.

> Both ELNES and EXELFS arise because the ionization process can impart more than the critical ionization energy (E_c) needed by the core electron to escape the attraction of the nucleus.

Any excess energy ($>E_c$) that the core electron possesses can be imagined as a wave emanating from the ionized atom. So again, we have to switch from a particle to a wave model of the electron, as we've done before, e.g., when we talked about diffraction in Part II. If this wave has only a few eV of excess energy, it undergoes plural elastic scattering from the surrounding atoms, as shown schematically in Figure 40.1A; this scattering is responsible for the ELNES, as we'll show. If the wave has even more excess energy, then it is less likely to be scattered several times and we can approximate the cause of the EXELFS to a single-scattering event, as shown in Figure 40.1B. Thus, EXELFS and ELNES can be viewed as a continuum of electron-scattering phenomena, with the arbitrary distinction that ELNES is confined to a few tens of eV past the edge onset. While ELNES arises from a more complex process than EXELFS, it is more widely used, because the ELNES is more intense, and so we'll discuss it first.

40.1.A. ELNES

The Physics: A core electron may receive enough energy from the beam electron to be ejected, but not enough to escape to the vacuum level. So it is still not free of all specific nuclear attraction. In such circumstances, the final state of the core electron will be in one of a range of possible energy levels above the Fermi energy (E_F). You may recall that the Fermi level, or the Fermi surface in three dimensions, is the boundary between the filled states and the unfilled states in the weakly bound conduction/valence bands (although, strictly speaking, this statement is only true when $T = 0$ K). In a metal, there is no separate valence band and E_F sits somewhere in the conduction band, as shown schematically in the classical energy level diagram of an atom in Figure 40.2. In an insulator or a semiconductor, E_F is between the valence band (which has all filled states) and the conduction band (which has no filled states).

The EELS: The excited electron can reside in any of the unfilled states, but not with equal probability. Some empty states are more likely to be filled than others because there are more states within certain energy ranges than in others. This uneven distribution of electron energy levels is termed the density of states (DOS) and this is also shown in the right diagram in Figure 40.2. Because of the greater probability of electrons filling certain unoccupied states above E_F, the intensity in the ionization edge is greater at the corresponding energy losses above the critical ionization energy E_C (which is equivalent to E_F), as shown in Figure 40.3.

> This variation in intensity, extending several tens of eV above E_C, is the ELNES and is effectively a probe of the DOS above E_F.

The Application: The importance of ELNES is that the DOS is extremely sensitive to changes in the bonding, or the valence state, of the atom. For example, if you look ahead to Figure 40.5 the carbon K ELNES is different for graphite and diamond and the Cu L ELNES changes when Cu is oxidized to CuO. On an even more detailed level, we can deduce the coordination of the ionized atom from the shape of the ELNES.

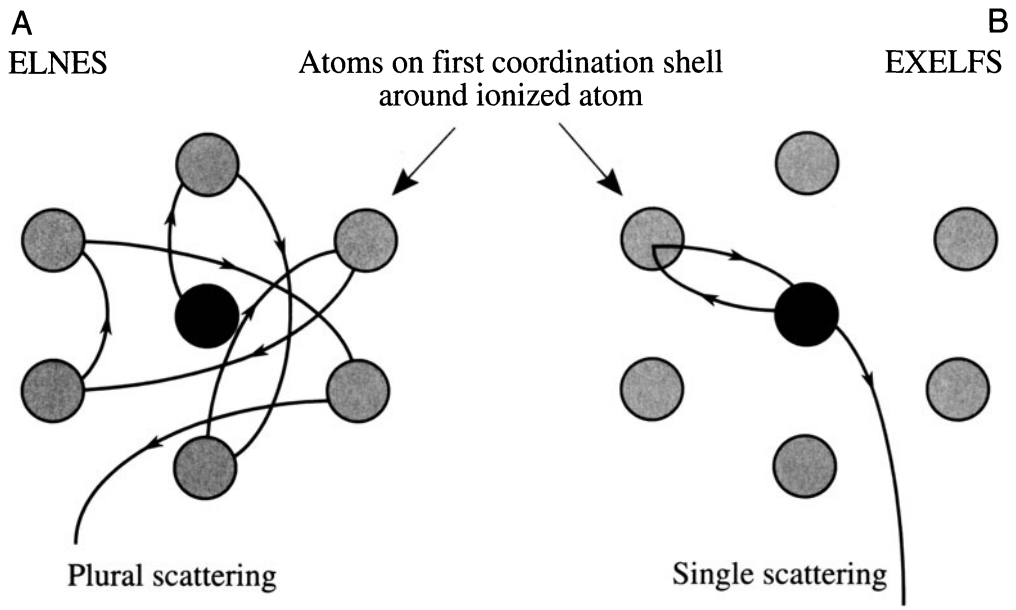

Figure 40.1. Schematic diagram showing the source of (A) ELNES and (B) EXELFS. The excess energy above the ionization threshold creates a wave radiating from the ionized atom which is scattered by surrounding atoms. The low-energy ELNES arises from multiple scatter and is affected by the bonding between the atoms. The higher-energy EXELFS approximates to single scatter and is affected by the local atomic arrangement.

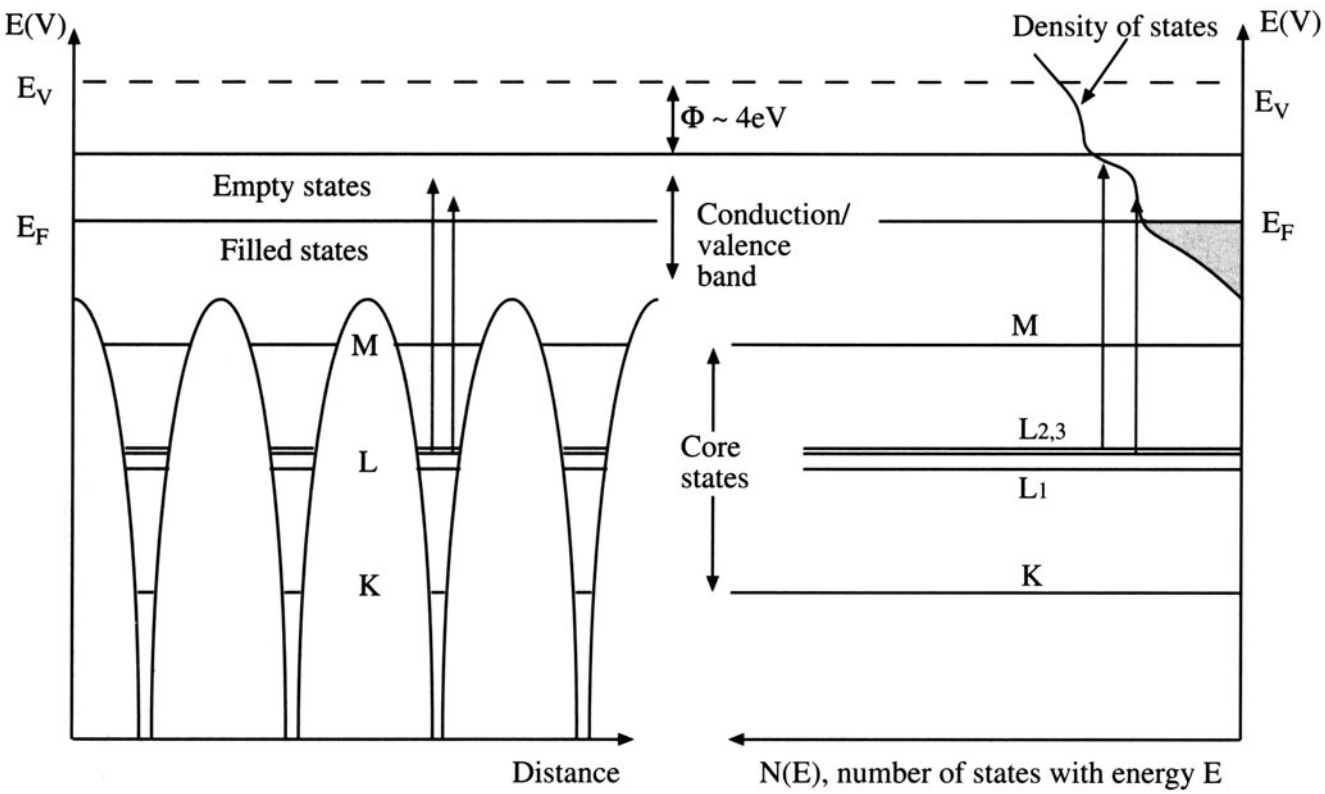

Figure 40.2. Relationship between the classical energy diagram of a metal atom (left) and the density of filled (shaded) and empty (unshaded) states (DOS) in the conduction band (right). The DOS is approximately a quadratic function on which small variations are superimposed. Ionization results in electrons ejected from the core states into empty states above the Fermi level (E_F).

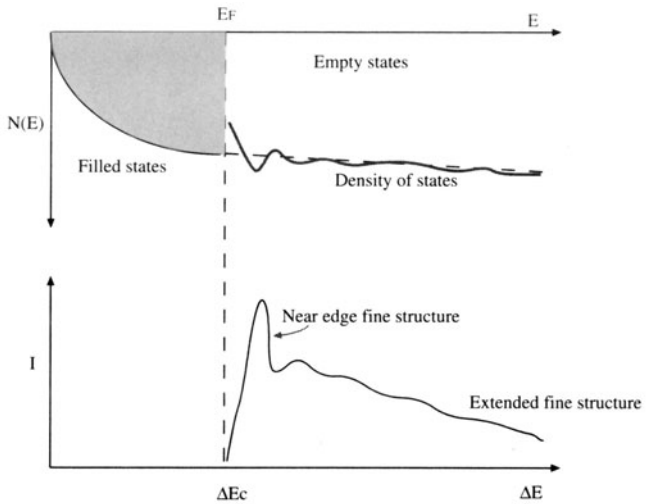

Figure 40.3. Relationship between the empty DOS and the ELNES intensity. Note the equivalence between the Fermi energy E_F and the ionization edge onset E_C. Electrons ejected from the inner shells reside preferentially in regions of the DOS with the greatest density of empty states. The filled states below E_F are shown as a quadratic function, but this is an approximation.

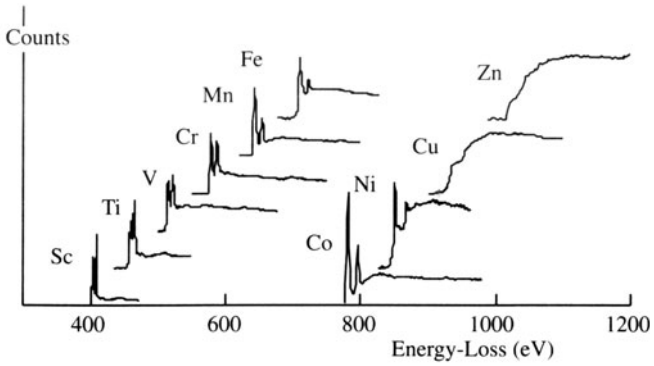

Figure 40.4. The L_3 and L_2 white lines in spectra from the transition metals show a slow variation in intensities until Cu, which has no white lines because the d shell is full.

Even if you don't understand the intricacies of the DOS and Fermi surfaces, you can still deduce bonding information simply by comparing your experimental ELNES with that from standard specimens of known valence state or coordination.

The EELS Atlas, which we've already referred to several times, contains many oxide spectra as well as elemental ones.

Perhaps the most startling example of ELNES is the presence of the "white lines," which we introduced in Section 38.4. They are intense sharp peaks on certain ionization edges; the L edges of the transition metals show such lines. Reminder: white lines were first seen on photographic plates in early X-ray absorption spectroscopy experiments. The white lines in the transition metal L edges are the L_3 and L_2 edges, respectively, as shown in Figure 40.4A. We'll explain what happened to L_1 later. To explain these lines we need a little more quantum physics, which you can skip if you wish and go to the last paragraph of this section. You should also be aware that there is disagreement as to whether white lines are truly "fine structure" or strictly ionization edge (atomic) intensity; but we'll not discuss this somewhat arcane argument.

More Physics: First, go back and look at Figure 38.4 to remind yourself that the various electron energy levels, K, L, M, etc., correspond to principal quantum numbers (n) equal to 1, 2, 3, etc. Within those energy levels, the electrons may have s, p, d, or f states, for which the angular momentum quantum number (ℓ) equals 0, 1, 2, 3, respectively. The notation s, p, d, f comes from the original description of the atomic spectral lines arising from these electron states, namely, sharp, principal, diffuse, and fine, although these have no counterpart in the EELS spectra we obtain.

As we noted in Section 38.4, the nomenclature $L_{2,3}$ arises from the fact that the L shell, from which the electron was ejected, has different energy levels. Such separation of the energies of the core states is called spin–orbit splitting.

Because the L electrons in levels 2 and 3 are in the p state, quantum theory demands that the sum (j) of their spin quantum number (s) and angular momentum quantum numbers (ℓ) is governed by the Pauli exclusion principle such that j (= s+ℓ) can only equal 1/2, 3/2, 5/2, etc. The spin quantum number, s (not to be confused with the s state), can only equal ±1/2. Taking all this into account along with other quantum number restrictions, it turns out that in the higher-energy (more tightly bound) L_2 shell we can have 2 p electrons with j = ±1/2 while in the L_3 shell we can have 4 p electrons with j = ±1/2, ±3/2. Therefore, we might expect twice as many electrons to be excited from the L_3 shell as from the L_2 shell, giving an L_3/L_2 intensity ratio of 2. While this rule is approximately obeyed in the Fe spectrum only, in practice the ratio is seen to increase along the transition metal series from 0.8 for Ti to 3 for Ni, as is also seen in the spectral sequence in Figure 40.4.

Now these p-state electrons in the L shell cannot be excited to just any unoccupied state.

The change $\Delta\ell$ in the angular momentum quantum number between the initial and final states must equal ±1. This constraint is called the *dipole selection rule.*

So for the p state ($\ell = 1$) the only permitted final states are either an s state ($\ell = 0$) or a d state ($\ell = 2$). Consequently, the electrons go up primarily into the unoccupied d states, since there are very few unfilled s states in the conduction band.

It is because of the dipole selection rules that we don't see a strong L_1 edge in the spectrum. The L_1 edge sits closer to the nucleus than the L_2 and L_3 edges and its electrons are in the s state ($\ell = 0$) so they can only be excited to a p state ($\ell = 1$), but not to a d state ($\ell = 2$), or to another s state. Since there are few unfilled p states in the conduction band of transition metals and they are much more spread out in energy than the d states, the L_1 intensity is very low and the peak is broad and may be invisible in the $L_{2,3}$ post-edge structure.

In fact, the energy width of the white lines is also affected by the time it takes for the ionized state to decay. One form of Heisenberg's uncertainty principle states that $\Delta E \Delta t = h/4\pi$, so a rapid decay gives a wide peak. For example, the Fe L_2 ionization can be rapidly compensated by an electron from the L_3 shell filling the hole and ejecting an Auger electron from the d shell. (This is called a Coster–Kronig transition.) A conduction-band electron could also fill the L_2 core hole, but the L_3 core hole can *only* be filled from the conduction band. Therefore, because there are two possible ways to fill the L_2 core hole, the L_2 line has a shorter Δt and a larger ΔE than the L_3 line, which is much sharper.

Back to Applications: So let's see how all of this can be useful. If you look at Figure 40.5A you'll see the carbon K edges for graphite and diamond. The carbon atom has hybridized s and p orbitals (termed σ and π in molecular-orbital theory). Graphite contains sp^2 bonds in the basal plane with van der Waals bonding between the planes. The diamond structure, in contrast, has four directional hybridized sp^3 covalent bonds. In diamond, atoms are tetrahedrally coordinated rather than arranged in graphite sheets. The strong peak on the rising portion of the K edge identifies the empty π^* states into which the K-shell electrons are transferred in graphite, while the diamond K edge has no such peak. This kind of information is extremely useful in the study of thin diamond and diamond-like carbon films, which are of tremendous current interest to both semiconductor manufacturers and the coatings industry. Carbon films can be made with a continuous range of graphitic and diamond-like character and it is possible to deduce the relative fraction of sp^3 (diamond) and sp^2 (graphite) bonding from the K-edge ELNES (Bruley *et al.* 1995). Another useful example is given in Figure 40.5B, where the changes in the Cu $L_{2,3}$ edge with oxidation are shown. This is a classical example, since Cu metal has all its 3d states filled so there are no white lines in spectra from the metal. Upon oxidation, some 3d electrons are transferred to the oxygen, leaving unfilled states, and the white lines appear in the oxide spectrum. Note also that the onset of the oxide edge is

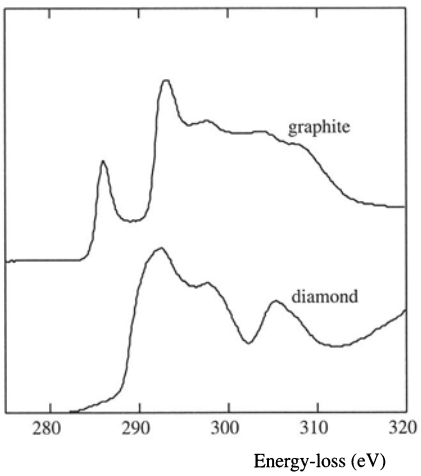

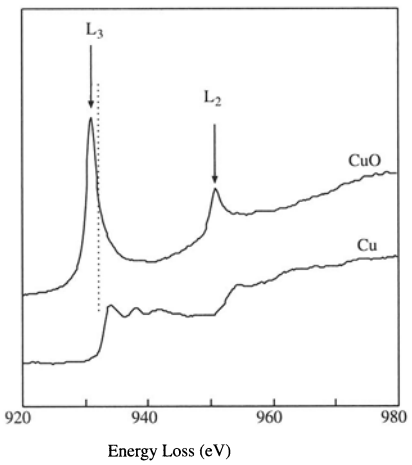

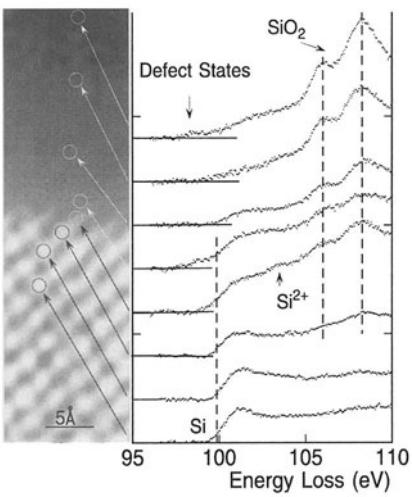

Figure 40.5. (A) Differences between the ELNES of the carbon K edge from graphite and diamond, (B) change in the Cu L edge as Cu metal is oxidized, (C) change in ELNES of the Si $L_{2,3}$ edge in a series of spectra gathered from individual atom rows across the interface between crystalline Si and amorphous SiO_2.

different from that of the metal, because this electron transfer changes the value of E_C.

This phenomenon is called a chemical shift and also helps to fingerprint the specimen.

Finally, in Figure 40.5C the Si L edge ELNES is seen to change across a Si-SiO_2 interface because the Si bonding changes. In this example, you can see the extraordinary power of an FEG STEM to provide simultaneous atomic-level images and spectra localized to individual atomic columns.

The combination of *Z*-contrast imaging (see Section 22.4) and PEELS is arguably the most powerful analytical technique for atomic characterization (see, e.g., Batson 1995, Browning and Pennycook 1995).

ELNES Calculations: Many attempts have been made to compare the ELNES with calculations of the density of states in simple materials such as metals and oxides. While the experimental and calculated spectra show reasonable agreement in terms of the energy of the various spectral features, there are still some discrepancies in the measured and calculated intensities. Great strides have been made in the last few years, mainly in improvements in models of the atomic potentials and in the computing power needed to pursue the calculations. This aspect is transforming the study of ELNES from an esoteric field to one with broad applications in materials science. There are two approaches to calculating the ELNES:

- Calculate the band structure directly in reciprocal space.
- Calculate the effect of multiple scattering of the electron wave in real space using the model shown in Figure 40.1A.

It can be shown that in fact these two approaches are mathematically equivalent. We'll emphasize the latter method since it is more commonly used.

Various approximations are made in ELNES modeling. The most critical approximation arises from the choice of the atomic potential. A common choice is the so-called "muffin-tin potential" in which a constant potential is assumed in the regions between atoms that don't touch. The potential within the atom must be spherically symmetrical. This model modifies the classical energy diagram, as shown in Figure 40.6. Apparently, this energy profile approximates to a cross section of a tin used by physicists to bake muffins. The potential profile across dissimilar adjacent atoms is asymmetrical, as also shown in Figure 40.6.

Having chosen a potential, the ELNES is determined by calculating all possible inter- and intra-shell scattering events suffered by the electron after it emerges above the Fermi level. A similar calculation is made in X-ray absorption near-edge structure (XANES) studies, and the two phenomena are equivalent. The wavelength is governed by the excess electron energy ($\mathcal{E}$-E_F). If the wavelength is long (i.e., low energy), the electron is scattered many times by the first few shells of atoms surrounding the ionized atom. One of the problems that confuses the issue is that the ion-

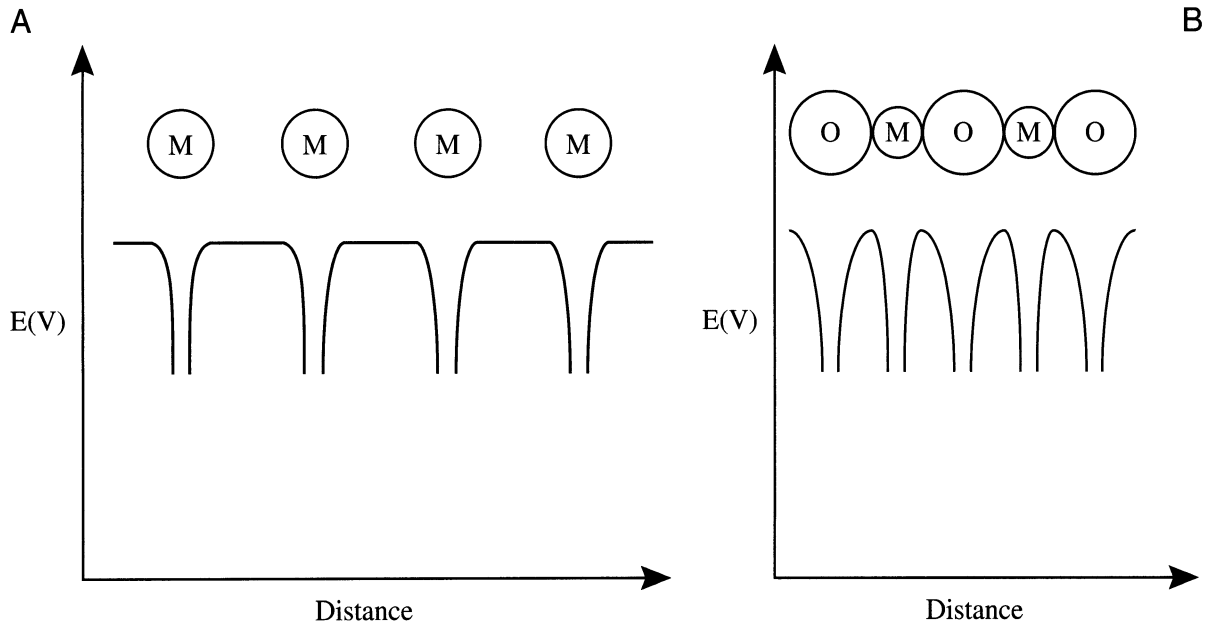

Figure 40.6. The muffin-tin potential energy diagram for (A) a non-closed-packed metal and (B) a metal oxide. Note the symmetry of the potential wells for the metal and the asymmetry for the oxide.

ization event results in a hole in the core shell, thus changing the atomic potential. This is called the *core-hole effect*, and it is accounted for by approximating the ionized atom to one with a nuclear charge of $Z+1$, since the missing electron lowers the shielding effect of the core electrons.

In ceramics and semiconductors the ionized electron remains localized to the ionized atom and may interact with the hole creating an electron-core hole bound state, termed an exciton. Creation of an exciton may influence the ELNES, although this remains a matter of some debate.

It can be shown that the multiple-scattering calculations predict modulations to the intensity of the ionization edge that correspond directly to the DOS of the ionized atom. So you should be aware that these calculations are only an *interpretation* of what actually happens to the electron after it emerges above the Fermi level.

Figure 40.7 shows a comparison of the calculated and theoretical ELNES for the Al L edge in tetrahedral and octahedral coordination in spinels. The difference due to different coordination is obvious. The sharp peak at the Al L-edge onset is thought to be an exciton. This effect is not well modeled by the theory, which otherwise makes a good match with the experimental data. The seminal paper in the field of ELNES experiments on transition metals and oxides is by Leapman *et al.* (1982), and a concise summary was given by Brydson (1991).

40.1.B. EXELFS

If the ejected electron does not fill an empty state, then its excess energy can also be interpreted as an electron wave

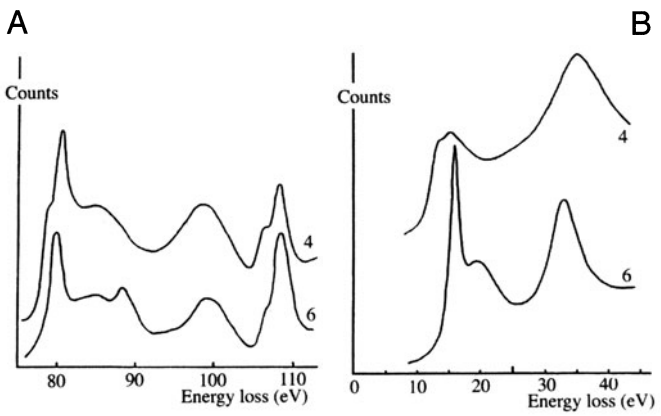

Figure 40.7. Comparison of (A) experimental spectra and (B) theoretical ELNES calculations for the Al $L_{2,3}$ edge in tetrahedrally coordinated (CN-4) and octahedrally coordinated minerals (CN-6). The calculated energy axis in (B) refers to eV above the L edge onset of ~75 eV.

which can be diffracted by the surrounding atoms in the structure, giving rise to EXELFS. Because the electron has higher energy than those which gave rise to ELNES, the diffraction is assumed to be single scattering, as shown in Figure 40.1B. As with any diffraction event, there is information about atomic positions in the EXELFS.

So ELNES is multiple scattering and EXELFS is single scattering, although the two phenomena overlap since the L_1 ELNES peak is often far enough past the edge onset to be included in the EXELFS.

The EXELFS modulations are each 20–50 eV wide (just visible in Figure 40.8A), and continue for several hundred eV. EXELFS is exactly analogous to the oscillations seen in the extended X-ray absorption edge fine structure (EXAFS) in synchrotron X-ray spectra. However, EXAFS results from complete photoabsorption of the incident X-ray while EXELFS involves absorption of only a small fraction of the energy of the beam electron.

Experimentally, it's not easy to see the EXELFS modulations because they are only about 5% of the edge intensity, and so you need good counting statistics. With SEELS you may have to gather the spectrum for many minutes or even hours, so PEELS is the only realistic way to pursue EXELFS. A thermionic source is probably best because it can deliver more current than an FEG; for this application, energy resolution is often less important. TEM diffraction mode will also increase your total signal intensity. Either way, you pay a price in terms of a loss of spatial resolution and an increased chance of specimen damage. If you need the best spatial resolution, an FEG and STEM mode is best.

We're interested in EXELFS because of the structural information contained in the intensity oscillations. To extract this information, you can use the Gatan ELP software (see Section 1.5), but you first have to ensure that the spectrum contains single-scattering information only, otherwise the plural-scattering intensity may mask the small EXELFS peaks.

Deconvolution is always the first step if the specimen isn't thin enough, i.e., if the plasmon peak is greater than 10% of the zero-loss peak.

Next, you have to remove the background if it wasn't done prior to deconvolution. Then the EXELFS intensity modulations are fitted to a smooth curve, and the intensity either side of the curve is plotted in **k** space (reciprocal space) (Figure 40.8B)

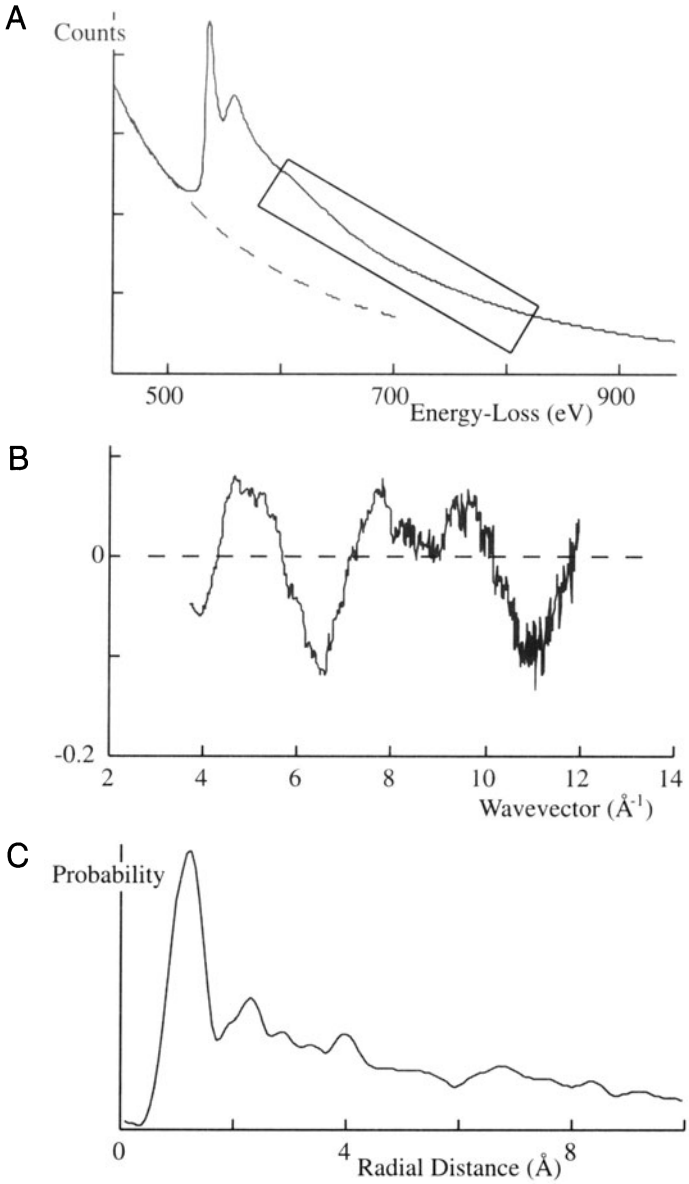

Figure 40.8. (A) EXELFS modulations are barely detectable in the selected post-edge region of an ionization edge. (B) The oscillations either side of a curve fitted to the post-edge spectrum are plotted in k space before (C) Fourier transforming the data to produce a radial distribution function.

$$k = \frac{2\pi}{\lambda} = \frac{[2m_0(E - E_K)]^{\frac{1}{2}}}{h} \qquad [40.1]$$

where E_K is the edge onset energy, E is the energy of the ejected electron, of wavelength λ, and the rest of the terms have their usual meaning. The electron wave interference gives periodic intensity maxima in **k** space when

$$\left(\frac{2a}{\lambda}\right)2\pi + \Phi = 2\pi n \qquad [40.2]$$

Here a is the distance from the ionized atom to the first scattering atom, and Φ is the phase shift that accompanies the scattering. Therefore, there are periodic maxima occurring for n = 1, 2, etc., and for different interatomic spacings. Consequently, you should be able to determine the local atomic environment, if the various interferences can be discriminated. The atomic spacing is obtained by a Fourier transform of the **k**-space modulations to give a radial distribution function, originating at the ionized atom (Figure 40.8C). Peaks in the RDF indicate the probability of an atom occurring a certain distance from the origin.

With EXELFS we can determine the partial RDF around a specific atom, and we are not restricted to the heavier atoms (Z >18) needed for EXAFS. So there is great potential for studying materials such as low-Z glasses, amorphous Si, and quasicrystalline structures. The high spatial resolution is obviously advantageous and all the data can be compared with diffraction patterns and images of the analyzed area. However, like all EELS techniques, we can't get good EXELFS unless the specimen is very thin. Despite these advantages, RDF work continues to be dominated by synchrotron sources because of the intensity of the signal, but EXELFS studies are increasing, e.g., Sklad *et al.* (1992), Qian *et al.* (1995).

RDF data acquired through EXELFS complement another TEM method of acquiring RDF information. This involves energy filtering of SAD patterns by scanning the pattern across the entrance aperture to the PEELS using post-specimen scan coils (Cockayne *et al.* 1991; see also Sections 18.6 and 40.3). Effectively, a full spectrum is available at each scattering angle but, in fact, only the zero-loss (ideally only the elastic) electrons are required. The plot of the zero-loss intensity as a function of scattering angle constitutes a line profile across a filtered diffraction pattern from which the RDF can be extracted; you can see a related example if you look ahead to Figure 40.15. This process does not have the spatial resolution of EXELFS, since typical SAD patterns are integrated over ~0.2–1 μm^2, but the signal is much stronger than EXELFS. Accuracies of ±0.001 nm in nearest-neighbor distances can be obtained, and the process is rapid enough to be performed on-line.

The techniques of ELNES and EXELFS are really quite remarkable demonstrations of quantum theory and the wave-particle duality. Consider that within the spectrum we are only gathering beam electrons that have been scattered by the specimen atoms, yet we are able to deduce information about what happened to those atoms *after* the beam–specimen interaction and where the atoms are in the structure!

An approximate particle-based analogy would be to imagine that we are catching bowling balls that have been thrown at pins, arranged in a certain pattern. (Although instructive, this exercise is best carried out as a thought experiment!) From the velocity of the balls that we catch, we are able not only to identify the weight of the pin that was hit (i.e., identify the characteristic ionization edge), but also to deduce how the pin fell down and where it rolled (the ELNES). Furthermore, we can also work out the spatial arrangement of the surrounding pins that didn't fall down (the EXELFS).

So how does the beam electron know where the core electron went after it left the core shell? The answer lies in the fact that the bowling ball (particle) analogy is totally inadequate. In fact, only certain electron transitions are allowed and the beam electron can therefore only transfer certain quantized energies to the core electron, not a continuum of possible energies. So the beam electron does know the possible final state of the core electron.

40.2. THE LOW-LOSS SPECTRUM

40.2.A. Plasmon Losses

The low-energy plasmon-loss region of the spectrum also contains chemical information, because the composition of the specimen may affect the free-electron density, n, which in turn changes the plasmon-energy peak position, since the two are related, as we described back in equation 38.6. Historically, this technique was the first aspect of EELS to produce quantitative microanalysis data, and it has been used in a limited number of systems, mainly aluminum and magnesium alloys in which the plasmon-loss spectrum is dominant and consists of sharp Gaussian peaks. For a review see Williams and Edington (1976).

The principle of plasmon-loss microanalysis is based on empirical observation of the shift in the plasmon peak position ($\mathcal{E}_P$) with composition (C), giving an expression of the form

$$\mathcal{E}_P(C) = \mathcal{E}_P(0) \pm C\left(\frac{d\mathcal{E}_P}{dC}\right) \qquad [40.3]$$

where $\mathcal{E}_P(0)$ is the plasmon energy loss for the pure component. By creating a series of binary alloys of known composition we can develop a working curve, which we can then use to calibrate measurements of $\mathcal{E}_P$ in unknown alloys. Table 40.1 summarizes the available plasmon-loss data for Al alloys, gathered in this manner.

Table 40.1. Alloys in Which the Variation of Plasmon Energy Loss $\mathcal{E}_p$ Has Been Measured as a Function of Composition

Alloy (at. %)	Range	$\mathcal{E}_p$ (eV) variation with fractional concentration C
Al-Mg	0–100	$\mathcal{E}_p = 15.3 - 5.0\ C_{Mg}$
Al-Mg	0–8	$\mathcal{E}_p = 15.3 - 4.4\ C_{Mg}$
Mg-Al	0–9	$\mathcal{E}_p = 10.61 + 5.9\ C_{Al}$
Al-Cu	0–2	Nonlinear
Al-Cu	0–2	$\mathcal{E}_p = 15.3^a - 10\ C_{Cu}$
Al-Cu	0–17.3	$\mathcal{E}_p = 15.3 + 4.0\ C_{Cu}$
Al-Zn	0–30	$\mathcal{E}_p = 15.3 - 0.2\ C_{Zn}$
Al-Ag	0–6	$\mathcal{E}_p = 15.3^a + 1.6\ C_{Ag}$
Al-Li	0–25	$\mathcal{E}_p = 15.3^a - 4.0\ C_{Li}$
Al-Ge	0–10	$\mathcal{E}_p = 15.3 + 0.1\ C_{Ge}$
Al-Zn-Mg	0–4	$\mathcal{E}_p = 15.3 - 4.7\ C_{Mg}$

[a]Normalized to 15.3 eV energy loss for pure Al.

Since plasmon-loss analysis demands the measurement of peak *shifts* rather than peak positions, you need an energy spectrum of the highest resolution and sufficient dispersion to measure the peak centroid accurately. The early plasmon-loss studies did not have access to FEGs and so the resolution of the thermionic source was a limiting factor. The poor resolution was compensated for to some extent by utilizing a high-dispersion Wien Filter or a Möllenstedt electrostatic spectrometer and recording the spectra photographically. More recently, similar results have been achieved using the relatively low-dispersion magnetic-prism spectrometer and electronic recording, but with an FEG. While the shift in the position of the plasmon peak may be as small as ~0.1 eV, the position of the peak centroid can still be measured to an accuracy of ~0.05 eV by computerized peak-fitting (Hunt 1995). Figure 40.9 illustrates some early plasmon-loss concentration data and the visible peak shifts that occur.

Plasmon-loss spectrometry has high spatial resolution and is relatively insensitive to specimen thickness and surface deposits. The spatial resolution is controlled by the localization of the plasmon oscillation, which is only about 10 nm, since the plasmon disturbance is rapidly damped in the free-electron gas. Your specimen thickness only affects the number and intensity of the plasmon peaks, not their position, as we described back in Figure 38.2. In fact, you get the best results from plasmon-loss spectrometry when your specimen is about 1–2 mean free paths (λ_P) thick, so that several intense Gaussian peaks are observable. The plasmon signal is intense and is the dominant loss feature in the spectrum. There are unfortunately strong practical disadvantages, which account for the almost complete absence of plasmon-loss data since the advent of ionization-loss techniques in the mid-1970s.

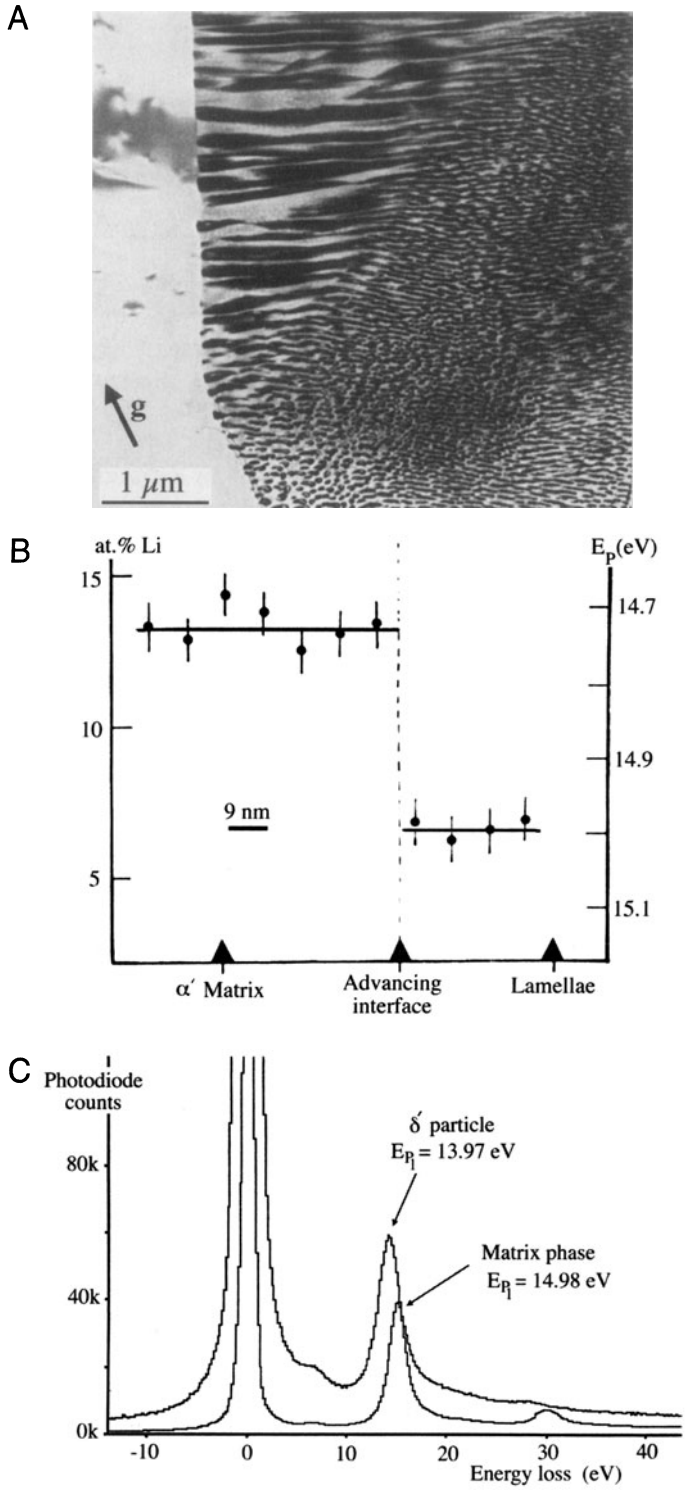

Figure 40.9. (A) Discontinuous transformation interface in Al-11 at.% Li. (B) Plasmon-loss variation and related Li composition change across the interface in (A). (C) Comparison of spectra from the matrix (5 at.% Li) and the precipitate (25 at.% Li) reveals the shift in the plasmon peak.

We are limited to specimens showing well-defined peaks, and only binary specimens can be sensibly analyzed.

In addition, the alloying element must produce a detectable change in $\mathcal{E}_p$ and this is by no means always the case. For example, the addition of 30 at.% Zn to Al scarcely changes $\mathcal{E}_p$. It is possible that application of modern detection and data-processing techniques may improve the quality and ease of acquiring and analyzing plasmon-loss spectra. However, it is not clear that they will permit the technique to be expanded significantly past the limited range of materials to which it has already been successfully applied.

While quantitative plasmon-loss microanalysis is limited, you can still use the plasmon part of the spectrum to identify unknown phases by the technique of "fingerprinting," as we showed in Figure 38.3. The low-loss portion of the spectrum is often sufficiently distinctive for different compounds that, since suitable libraries of known spectra exist that we've already referenced, you can use these libraries to cross-check the spectra from unknowns. In fact the plasmon-loss spectrum is more robust than the ionization-loss spectrum, since it will not change significantly as you change such experimental variables as α, β, kV, and it is insensitive to the data-processing variables that plague ionization-loss spectra. For example, direct examination of the low-loss spectrum is sufficient to distinguish between free-electron metals and transition metals, as shown in Figures 40.10A,B. Similarly, the low-loss spectra of the different oxides are equally distinctive (Figure 40.10C).

40.2.B. Dielectric-Constant Determination

We can view the energy-loss process as the dielectric response of the specimen to the passage of a fast electron. As a result, your energy-loss spectrum contains information about the dielectric constant or permittivity (ε). The single-scattering spectrum intensity $I(\ell)$ is related to ε by the expression (Egerton 1996)

$$I(\ell) = I_0 \frac{t}{k} \mathrm{Im}\left(-\frac{1}{\varepsilon}\right) \ln\left|1 + \left(\frac{\beta}{\theta_E}\right)^2\right| \qquad [40.4]$$

where I_0 is the intensity in the zero-loss peak, t is the specimen thickness, and k is a constant incorporating the electron momentum and the Bohr radius. You can use a Kramers–Kronig analysis to analyze the energy spectrum in order to extract the real part of the dielectric constant from the imaginary part (Im) in equation 40.4, and details

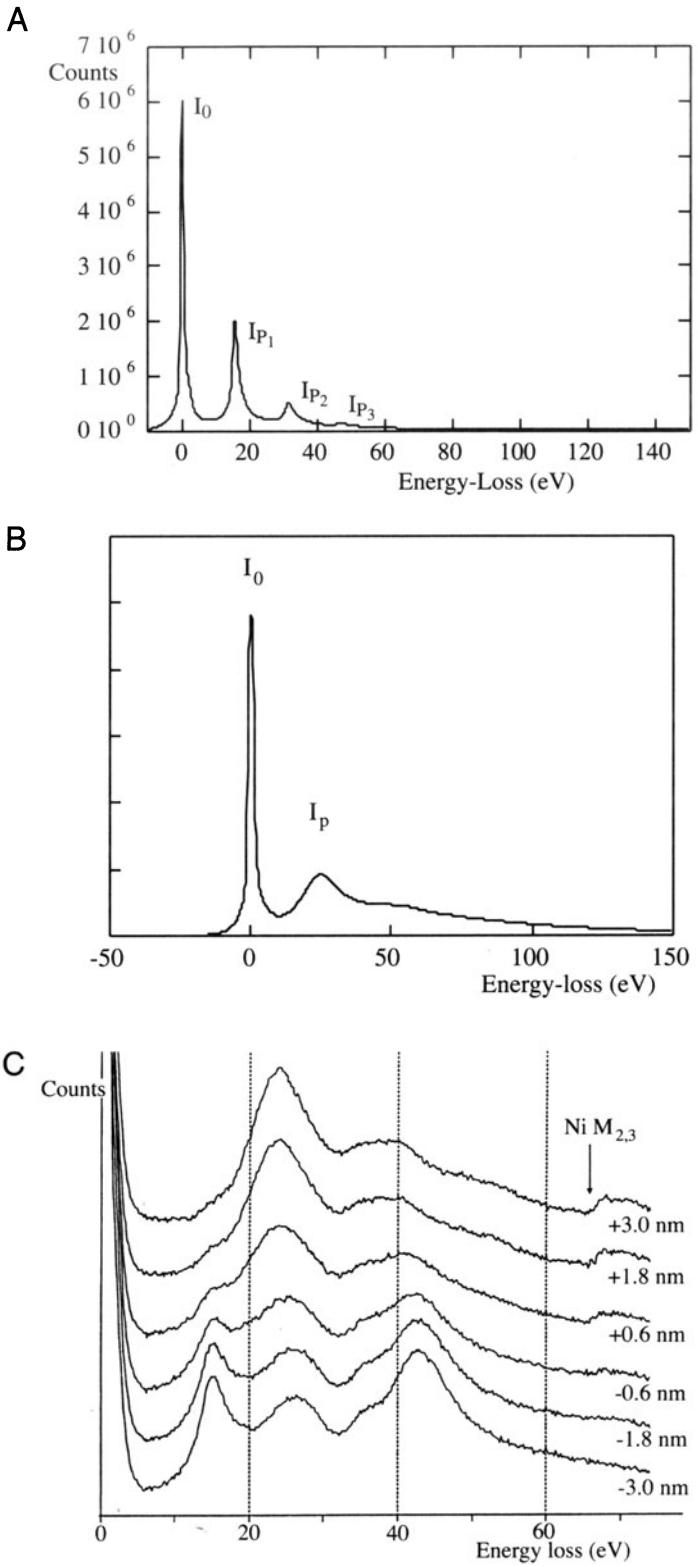

Figure 40.10. (A) Multiple plasmon peaks from Al, which is a free-electron metal, compared with (B) the single weak plasmon from a transition metal, Fe. (C) Six low-loss spectra taken across a NiO (top)–ZrO_2 (bottom) interface showing characteristic differences in the plasmon intensities which occurred within ±3 nm of the interface.

are given in Egerton (1996). Since you need a single-scattering spectrum, deconvolution is again the first step.

> The Kramers–Kronig analysis gives the energy dependence of the dielectric constant and other information which we usually obtain by optical spectroscopy.

The advantage of EELS for this kind of work is the improvement in spatial resolution over electromagnetic radiation techniques. Also, the frequency range which is available is more extended. The low-energy plasmon part of the energy-loss spectrum out to about 20 eV is of most interest to us, and corresponds to optical analysis of the dielectric response from the visible through the ultraviolet frequency range. So in a single EELS experiment you can, in theory, substitute for a whole battery of optical spectroscopy instrumentation. Physicists are most interested in the low-frequency range around 1 eV, since this is less accessible through optical spectroscopy. For this you need an FEG and a high-resolution spectrometer, and you need to deconvolute out the tail of the zero-loss peak so it does not mask the low-energy intensity. An example of the correspondence between EELS and optical dielectric constant spectra is shown in Figure 40.11.

40.2.C. Band-Gap and Interband Transitions

In the region of the spectrum immediately after the zero-loss peak, and before the rise in intensity preceding the plasmon peak, you can see a region of low intensity. If this intensity approaches the dark noise of the detector, then there are no electron–electron energy transfers occurring. This effect implies that there is a forbidden transition region, which is simply the band gap between the valence and conduction bands in semiconductors and insulators. Figure 40.12A illustrates the variable band gap from specimens of Si, SiO_2, and Si_3N_4. In this region there are sometimes small peaks that correspond to interband transition which require energy losses of <10 eV, and surface plasmons may occur. An example of an interband transition is given in the spectra from two polymers shown in Figure 40.12B.

40.2.D. Angle-Resolved EELS

Most of the time we've been talking about locating the beam at different positions on the specimen and gathering a spectrum by sending the direct beam into the spectrometer. This is often called "spatially resolved" EELS since spectra came from different spatial locations on the speci-

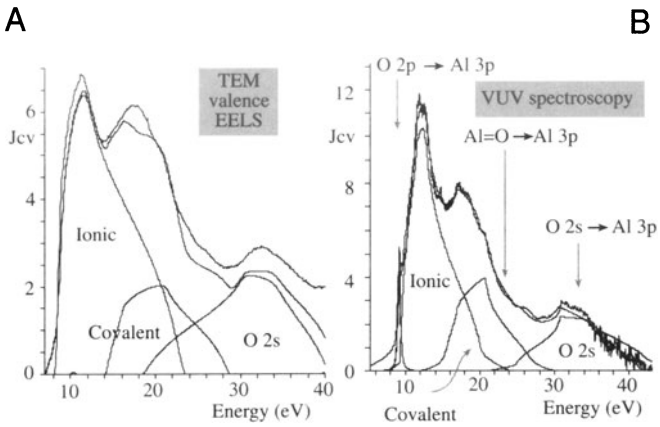

Figure 40.11. Comparison of thin-specimen EELS (A) and bulk-specimen optical dielectric constant data (B) for α-Al_2O_3. J_{cv} is the interband transition strength and the various transitions are labeled: transitions from the filled O 2p level represent ionic bonding, transitions from the hybridized Al=O level represent covalent bonding, interband transitions from O 2s–Al 3p are also detected. Individual contributions to the spectra have been obtained via a critical point model.

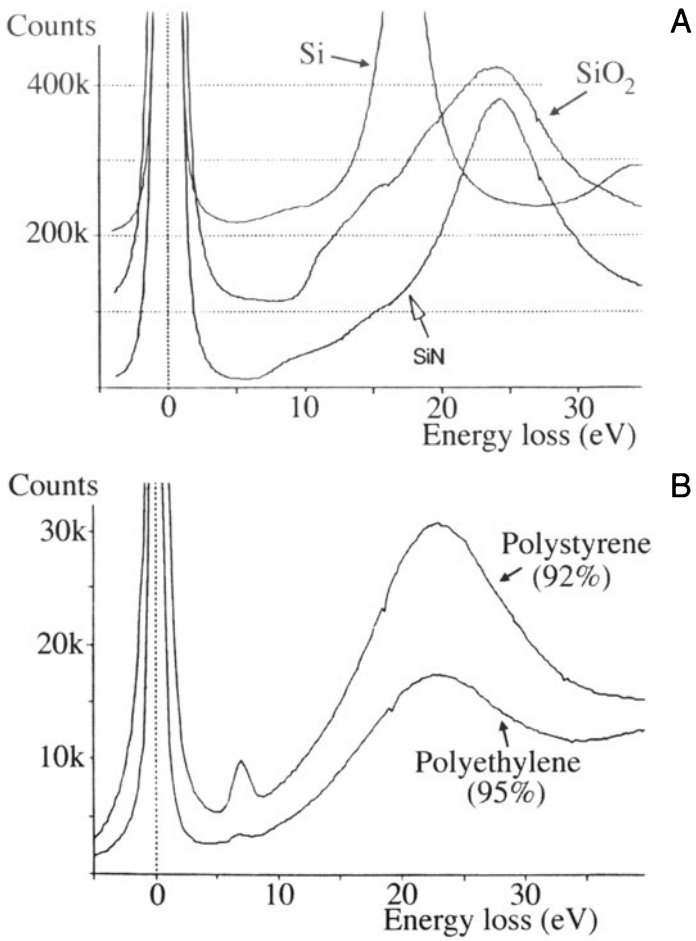

Figure 40.12. (A) Band-gap differences evident in the low-loss spectra of a Si semiconductor and SiO_2 and Si_3N_4 ceramic insulators. (B) The interband transition characteristic of polystyrene, clearly visible on the rise of the plasmon peak, compared with the absence of such a transition in polyethylene.

men. However, we have occasionally mentioned that the *angle* of scatter of energy-loss electrons is important, and there is a whole field of EELS research that studies angle-resolved spectra. To do this, we just scan the DP across the PEELS entrance aperture (or the SEELS slit) and gather spectra at different angles, as for RDF measurements that we just described. However, rather than studying the energy of electrons primarily, this technique emphasizes the determination of the *momentum* of the energy-loss electrons. Momentum transfer studies were pioneered by Silcox and co-workers (e.g., Leapman and Silcox 1979), and now with FEG STEMs you can get even more information about the symmetry of electronic states which complements spatially resolved ELNES (e.g., Wang *et al.* 1995).

One practical aspect of angle-resolved EELS is the study of Compton scattering, which is the ejection of outer-shell electrons by high-energy photons or electrons. We can detect these Compton-scattered electrons by observing the EELS spectrum at a high scattering angle (about 100 mrad), either by displacing the objective aperture to select an off-axis portion of the diffraction pattern or by tilting the incident beam. This process has been used to analyze the angular and energy distribution of Compton-scattered electrons and determine bonding information, since the Compton-scattering process is influenced by the binding energy (Schattschneider and Exner 1995).

You can appreciate now that there is a wealth of detail in the energy-loss spectrum beyond the basic chemistry of the specimen. To extract this information you need a single-scattering (deconvoluted) spectrum and sophisticated mathematical analysis. Often, our interpretation of the data is limited by lack of knowledge of the physics of the electron–specimen interaction. However, considerable research is going on into these aspects of EELS and these fine structure studies are the future of the technique.

40.3. ENERGY-FILTERED AND SPECTRUM IMAGING

We can select the intensity in any part of the EELS spectrum and use it to form an image, either in a digital manner by modulating the signal to the STEM screen or in an analog manner in the energy-selecting TEM. A variety of images can be formed in this way and they have several advantages over conventional TEM and STEM images. We will describe the experimental procedures first and then discuss the different types of images.

40.3.A. STEM Digital Imaging

In SEELS, the ramp voltage to the magnetic prism must be held at a constant setting, so only those electrons in the energy range accepted by the slit pass through the spectrometer. In PEELS you select the output from specific diodes. In either case you've used the spectrometer to select electrons of a fixed energy range. If these electrons are then allowed to hit a detector, the signal can be used to form energy-filtered images. In a TEM/STEM you use the signal from the EELS scintillator to modulate the STEM CRT, while in a dedicated STEM the BF detector sits beyond the EELS and so all your BF images are energy-filtered. To avoid image shifts due to scanning of the beam on the specimen, you must descan the beam using a set of post-specimen coils, which are usually present in the TEM or STEM column as a matter of course. In SEELS, if the spectrometer slit width is too large, your image will suffer from chromatic aberration because electrons of different energy are focused at different planes. In PEELS, the intensity is controlled by the total spectral-acquisition time per pixel. Here, an FEG is best if high-resolution images with reasonable pixel numbers are to be acquired.

With PEELS, it is possible to collect a spectrum in a sufficiently short time (< 50 ms) that you can create images in which a complete spectrum is stored at each pixel and all data processing is carried out after the acquisition.

Then we have what is known as a *spectrum image* (Jeanguillaume and Colliex 1989). Such images contain immense amounts of data and you need sophisticated hardware and software routines to handle the data. For example, a 512×512 pixel image with a full 1024 channel spectrum at each pixel contains more than 25 Mb of data. Because of the relatively long time to acquire spectrum images, drift correction and other PEELS corrections are necessary (Hunt and Williams 1991). Within such an image you have a *complete* record of the electron–specimen interaction and from such you can create multiple images, as shown in Figure 40.13. This figure is from an Al-Li alloy and shows the distribution of the component elements. There are three strong advantages to this approach:

- You can analyze the "specimen" at a later time, without putting it back in the microscope, and look for elements that were not initially thought to be present or to be important.
- You can process the data in several different ways to compare quantification schemes and the possibility of discerning unexpected correlations between elemental distributions.
- All the information in the EELS spectrum can be mapped discretely, creating, for example, not just elemental images, but dielectric-constant images, valence-state images, thickness images, etc.

40.3.B. TEM Analog Imaging

For analog imaging in a TEM, an Ω filter spectrometer sits between the first and second pairs of projector lenses, as shown back in Figure 37.11 for the LEO EM912. To select

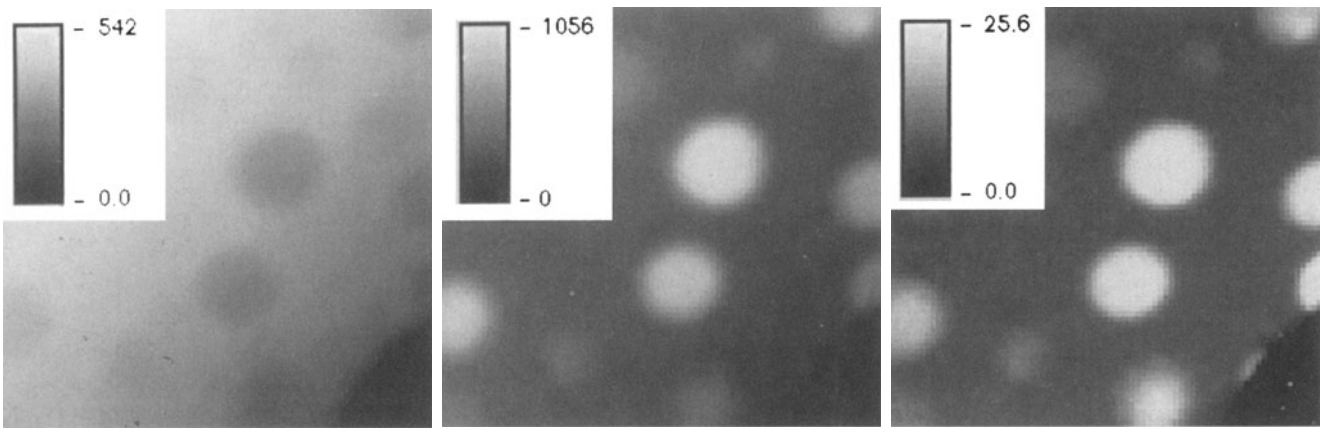

Figure 40.13. Three processed spectrum images of an Al-Li alloy aged to give a dispersion of δ′ precipitates. The left image shows the absolute concentration of Al (atoms/nm^2) obtained from quantification of the Al $L_{2,3}$ edge, the middle image is the absolute Li content (atoms/nm^2) from the Li K edge, and the right image is the Li content (at. %) obtained from the shift of the first plasmon peak. The inserts show the correlation between image intensity and the range of composition imaged.

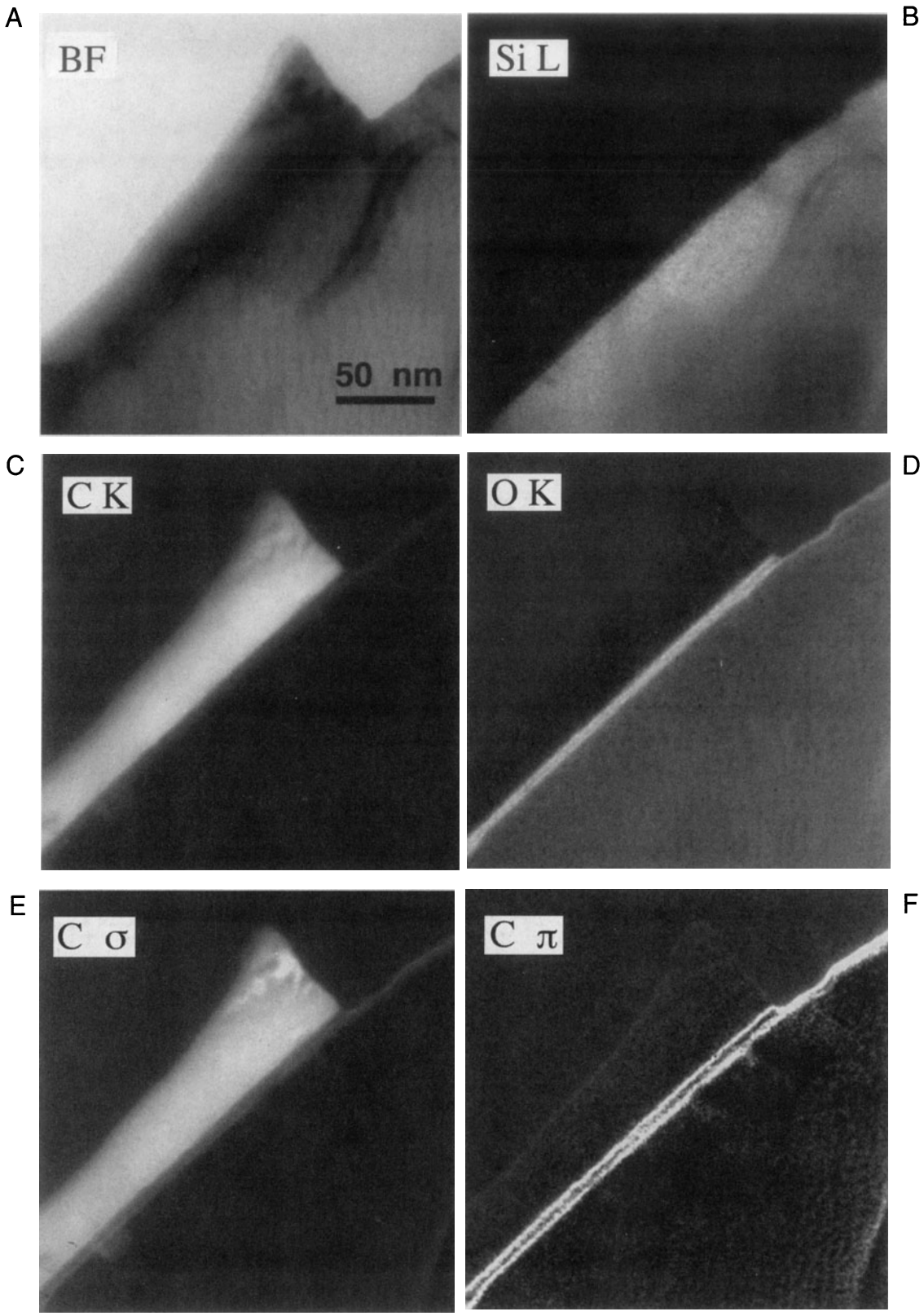

Figure 40.14. (A) TEM BF and (B–F) a series of electron spectroscopic images revealing the Si, C, and O elemental distributions and the carbon bonding maps at the interface between a diamond-like carbon film and a Si substrate. In the oxygen-rich amorphous layer at the interface the carbon atoms exhibit a double layer of π bonds while the carbon film itself is predominantly σ bonded, indicating a high degree of diamond-like character.

the electrons for this imaging (ESI), you shift the spectrum relative to the slit that is positioned after the filter but before the final projector lens. In the LEO instrument, you make the shift by increasing the accelerating voltage of the microscope by $+E$ in order to keep the energy-loss electrons of interest ($-\mathcal{E}$) on the optic axis; this shift correction is prealigned for the chosen kV. You can filter either an image or DP simply by changing the strength of the intermediate lens preceding the Ω filter. In addition, you can also see the energy-loss spectrum on the TEM screen. This method of spectral display has the advantage that the angular distribution of the energy-loss electrons is spatially resolved, although the absolute intensity has to be determined by digitizing the spectrum or using a microdensitometer. However, this is not the major mode of operation of the instrument, which is optimized for electron spectroscopic imaging (ESI), and many examples are given in a special issue of the *Journal of Microscopy* (Knowles 1994).

For ESI, you adjust the energy window by varying the slit width. With a 20-eV window you can obtain images with a chromatic-aberration limit of ~2.5 nm, which compares well with normal TEM C_c-limited resolution. Resolution may be as good as 0.5 nm under ideal conditions. You can select the area to image via a selected-area aperture, or by using Kohler illumination conditions, in which a small parallel beam of electrons is created.

A drawback to this ESI process is that, while background-subtracted core-loss images are easily obtainable, they are not quantitative if significant changes in specimen thickness occur.

However, the images can be acquired in a few seconds, rather than many minutes or hours for a digital image, and a range of filtered images are compared with a conventional TEM BF image in Figure 40.14A–F. ESI is equally applicable to diffraction patterns; energy-filtered CBED is a very powerful technique for extracting more data from conventional CBED patterns, as shown in Figure 40.15. Deininger *et al.* (1994) have demonstrated how energy-filtered CBED patterns can be used to determine structure factors, lattice strains, and the accelerating voltage of the TEM. Removing the inelastic electrons removes much of the diffuse scattering from your diffraction patterns, making comparison of experimental and simulated patterns much easier. In addition to energy-filtered CBED patterns, as shown in Figure 40.15, SAD patterns can be similarly sharpened up, and used for RDF determination, as we already mentioned in Section 40.1.B

In summary, you can perform EELS imaging in two very different ways in a TEM and STEM. You can obtain a variety of images, depending on which portion of your spectrum is selected and the nature of your specimen. The strong forward-scattered EELS signal, combined with close to 100% detection efficiency, means that EELS imaging is much more statistically viable than thin-film X-ray mapping. This fact, combined with the enormous number

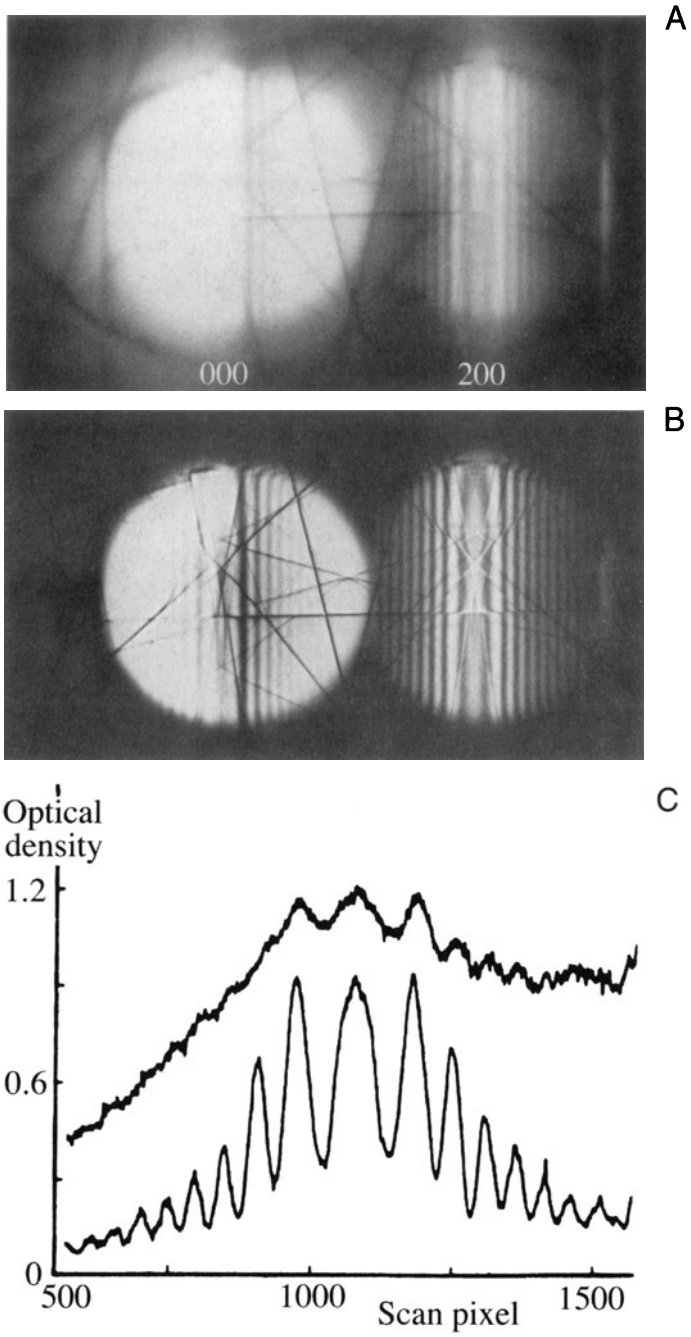

Figure 40.15. (A) Experimental CBED two-beam pattern (000 and 220) from a Si specimen, 270 nm thick. (B) The same pattern energy-filtered using the Zeiss Ω filter with an 8-eV window revealing the K-M fringes useful for thickness determination. (C) Densitometer traces across the 220 diffraction disk, unfiltered (above) and filtered (below).

of signals available in the EELS spectrum, make EELS imaging an extremely attractive technique.

Combination of energy filtering with conventional TEM imaging and diffraction will increase as the development of digital TEM technology continues. It is likely that all images will routinely be filtered to remove chromatic aberration effects, which will be a tremendous aid to the materials scientist struggling to make thin specimens from complex multiphase materials. As digital storage becomes cheaper, the ability to save complete spectrum images of all your specimens will become the norm, thus enhancing the claim that the TEM is *the* most versatile instrument for the characterization of materials.

As a final word, never forget to combine techniques wherever possible to characterize your material. If you are creative, you can even do simultaneous experiments, e.g., by constructing an STM in a TEM (Spence *et al.* 1990). We encourage you to experiment with the microscope at *all* opportunities. Don't think there is nothing new to discover; there is still ample room for you to exercise your imagination and innovation, and the TEM is a fascinating place in which to do just that.

CHAPTER SUMMARY

Both the experimental techniques and the theoretical understanding of EELS are still developing. We have introduced several specialized topics:

- Energy-loss near-edge structure (ELNES).
- Extended energy-loss fine structure (EXELFS).
- Low-loss fine structure.
- Angle-resolved (momentum transfer) EELS.
- Electron spectroscopic imaging (ESI) and spectrum imaging.

However, we have only given you a suspicion of the potential of these topics. If EELS becomes a technique you use in your research, or if you have the time, we recommend watching developments of the technique in the journals referenced at the end of this chapter. EELS, particularly fine structure and imaging, is one of the most dynamic areas of TEM development.

REFERENCES

General References

Egerton, R.F. (1996) *Electron Energy-Loss Spectroscopy in the Electron Microscope,* 2nd edition. Plenum Press, New York.

Raether, H. (1965) *Electron Energy-Loss Spectroscopy, Springer Tracts in Modern Physics,* Springer-Verlag, New York.

Teo, B.K. and Joy, D.C. (1981) *EXAFS Spectroscopy; Techniques and Applications,* Plenum Press, New York.

Specific References

Batson, P.E. (1995) *Ultramicroscopy* **59**, 63.

Browning, N.D. and Pennycook, S.J. (1995) *J. Microsc.* **180**, 230.

Bruley, J., Williams, D.B., Cuomo, J.J., and Pappas, D.P. (1995) *J. Microsc.* **180**, 22.

Brydson, R. (1991) *EMSA Bulletin* **21**, 57.

Cockayne, D.J.H., McKenzie, D., and Muller, D. (1991) *Microsc. Microanal. Microstruct.* **2**, 359.

Deininger, C., Necker, G., and Mayer, J. (1994) *Ultramicroscopy* **54**, 15.

Hunt, J.A. (1995) in *Microbeam Analysis-1995* (Ed. E.S. Etz), p. 215, VCH Publishers, New York.

Hunt, J.A. and Williams, D.B. (1991) *Ultramicroscopy* **38**, 47.

Jeanguillaume, C. and Colliex, C. (1989) *Ultramicroscopy* **28**, 252.

Knowles, K.M., Ed. (1994) *J. Microsc.* **174**, 131.

Leapman, R.D. and Silcox, J. (1979) *Phys. Rev. Lett.* **42**, 1362.

Leapman, R.D., Grunes, L.A., and Fejes, P.L. (1982) *Phys. Rev.* **B26**, 614.

Qian, M., Sarikaya, M., and Stern, E.A. (1995) *Ultramicroscopy* **59**, 137.

Schattschneider, P. and Exner, A. (1995) *Ultramicroscopy* **59**, 241.

Sklad, P., Angelini, P., and Sevely, J. (1992) *Phil Mag.* **A65**, 1445.

Spence, J.C.H., Lo, W., and Kuwabara, M. (1990) *Ultramicroscopy* **33**, 69.

Wang, Y.Y., Cheng, S.C., Dravid, V.P., and Zhang, F.C. (1995) *Ultramicroscopy* **59**, 109.

Williams, D.B. and Edington, J.W. (1976) *J. Microsc.* **108**, 113.